

# Local polar fluctuations in lead halide perovskite crystals

Omer Yaffe,<sup>1,\*</sup> Yinsheng Guo,<sup>1,\*</sup> Liang Z. Tan,<sup>2</sup> David A. Egger,<sup>3</sup> Trevor Hull,<sup>1</sup> Constantinos C. Stoumpos,<sup>4</sup> Fan Zheng,<sup>2</sup> Tony F. Heinz,<sup>5,6</sup> Leeor Kronik,<sup>3</sup> Mercuri G. Kanatzidis,<sup>4,7</sup> Jonathan S Owen,<sup>1</sup> Andrew M. Rappe,<sup>2</sup> Marcos A. Pimenta,<sup>1,8</sup> and Louis E. Brus<sup>1,†</sup>

<sup>1</sup>*Department of Chemistry, Columbia University, New York, NY 10027, USA*

<sup>2</sup>*Department of Chemistry, University of Pennsylvania, Philadelphia, Pennsylvania 19104, USA*

<sup>3</sup>*Department of Materials and Interfaces, Weizmann Institute of Science, Rehovoth 76100, Israel*

<sup>4</sup>*Materials Science Division, Argonne National Laboratory, Argonne, Illinois 60439, USA*

<sup>5</sup>*Department of Applied Physics, Stanford University, Stanford, CA 94305, USA*

<sup>6</sup>*SLAC National Accelerator Laboratory, Menlo Park, California 94025, United States*

<sup>7</sup>*Department of Chemistry, Northwestern University, Evanston, Illinois 60208, USA*

<sup>8</sup>*Departamento de Física, Universidade Federal de Minas Gerais, 30123-970 Belo Horizonte, Brazil*

(Dated: February 13, 2017)

Hybrid lead-halide perovskites have emerged as an excellent class of photovoltaic materials. Recent reports suggest that the organic molecular cation is responsible for local polar fluctuations that inhibit carrier recombination. We combine low frequency Raman scattering with first-principles molecular dynamics (MD) to study the fundamental nature of these local polar fluctuations. Our observations of a strong central peak in the cubic phase of both hybrid ( $\text{CH}_3\text{NH}_3\text{PbBr}_3$ ) and all-inorganic ( $\text{CsPbBr}_3$ ) lead-halide perovskites show that anharmonic, local polar fluctuations are intrinsic to the general lead-halide perovskite structure, and not unique to the dipolar organic cation. MD simulations indicate that head-to-head Cs motion coupled to Br face expansion, occurring on a few hundred femtosecond time scale, drives the local polar fluctuations in  $\text{CsPbBr}_3$ .

Keywords: Local polar fluctuations; Hybrid perovskites; Low frequency Raman scattering; molecular dynamics; radiation detection; Central peak;

Lead-halide hybrid perovskite crystals have emerged as promising materials for inexpensive and efficient solar cells. The rapid increase in solar cell power conversion efficiency [1, 2] provides impetus to gain fundamental understanding of the interplay between their electronic and structural properties.

Recent reports show that even without defects, hybrid perovskite crystals display significant structural fluctuations [3–14]. The organic molecular cation plays an important role in the structural fluctuations of the hybrid perovskites, as supported by dielectric measurements, neutron scattering, and molecular dynamics [15–18]. These studies revealed molecular dipole orientations fluctuating on a picosecond time scale, with the octahedral halide cages exhibiting large anharmonic thermal fluctuations in response. [19, 20] These large thermal polar fluctuations may result in local dynamic fluctuations of the electronic band gap and thus play a key role in determining electronic properties of hybrid crystals [4, 14, 21].

Here, we investigate the nature of this unique structural behavior by combining low-frequency Raman scattering with MD simulations. Our experimental approach is to conduct a comparative study of  $\text{CH}_3\text{NH}_3\text{PbBr}_3$ , a hybrid perovskite, and  $\text{CsPbBr}_3$ , an all-inorganic halide perovskite with a similar band gap and structural phase sequence. [22, 23] We show that anharmonic effects [18]

are not limited to hybrid perovskites with molecular cations, but are also present in the all-inorganic  $\text{CsPbBr}_3$ . In both  $\text{CH}_3\text{NH}_3\text{PbBr}_3$  and  $\text{CsPbBr}_3$ , we observe a “central” (zero-frequency) peak in their Raman spectra, which grows in prominence from a small background signal in the low temperature orthorhombic phases to the dominant spectral feature in the cubic phases. Such a central peak is a signature of local polar thermal fluctuations [24–26]. Raman central peaks do not arise in purely harmonic systems, which have well-defined Raman lines at finite frequencies. Instead, Raman central peaks are associated with polar correlations occurring over a range of time scales, which give rise to spectral weight over a continuum of frequencies. The presence of the central peak in both  $\text{CH}_3\text{NH}_3\text{PbBr}_3$  and  $\text{CsPbBr}_3$  shows that local polar fluctuations exist in both systems, even when the polar molecular cation  $\text{CH}_3\text{NH}_3^+$  is replaced by the atomic cation  $\text{Cs}^+$ . Using first-principles MD simulations, we assign the central peak in  $\text{CsPbBr}_3$  to anharmonic, head-to-head motion of Cs cations in the cubo-octahedral voids of the perovskite structure combined with the distortion of  $\text{PbBr}_6$  octahedra. These local polar fluctuations occur on the hundred femtosecond time scale.

We performed Raman scattering measurements on high quality  $\text{CH}_3\text{NH}_3\text{PbBr}_3$  and  $\text{CsPbBr}_3$  single crystals over a range of temperatures, thus probing for the orthorhombic, tetragonal, and cubic phases. Raman scattering spectra were obtained with excitation by 1.96 eV CW HeNe laser. By using this excitation energy, we benefit from a pre-resonance Raman effect where the scattering cross section is enhanced

\* These authors contributed equally

† leb26@columbia.edu

via proximity to the band gap optical transition.[27] Along with our Raman experiments, we compute theoretical Raman spectra of CsPbBr<sub>3</sub> from first-principles MD, based on density functional theory (DFT). These calculations were performed at 80 K and 500 K, using lattice parameters of the orthorhombic and cubic CsPbBr<sub>3</sub> unit cell [22], respectively, which were optimized with dispersion-corrected DFT [28](see supplemental material). We calculate semiclassical Raman spectra from the autocorrelation function of the polarizability obtained from first-principles [28]. In both the experimental and calculated Raman spectra, we observe a series of sharp peaks superimposed on a broad central peak exhibiting a highly temperature-dependent intensity. This agreement between spectroscopy and theory allows us to extract and identify the atomic motions responsible for the central peak in the Raman spectra.

In figure 1 we compare the Raman scattering spectra of CH<sub>3</sub>NH<sub>3</sub>PbBr<sub>3</sub> and CsPbBr<sub>3</sub> single crystals across their similar phase sequence (see supplemental material for x-ray diffraction data on phase sequence vs temperature for CH<sub>3</sub>NH<sub>3</sub>PbBr<sub>3</sub> [15, 29] and CsPbBr<sub>3</sub> [22, 30]). Note that the transition temperatures of CsPbBr<sub>3</sub> are much higher than those of CH<sub>3</sub>NH<sub>3</sub>PbBr<sub>3</sub>.

At 80 K, sharp, well-resolved Raman spectra are observed for CH<sub>3</sub>NH<sub>3</sub>PbBr<sub>3</sub> and CsPbBr<sub>3</sub> crystals (bottom-blue curves in Figures 1a and b, respectively). Both spectra share similar features: two strong modes below 50 cm<sup>-1</sup>, a set of three peaks around 70–80 cm<sup>-1</sup>, and a broad, low-intensity feature centered around 135 cm<sup>-1</sup>.

Unlike the low-temperature spectra, the Raman spectra in the tetragonal (Figure 1a,b, middle-green) and cubic (Figure 1a,b, top-red) phases are diffuse, composed of a central peak with a significant spectral continuum underlying broad Raman transitions at positions corresponding to modes modestly softened from the sharp 70 cm<sup>-1</sup> and 120 cm<sup>-1</sup> features presented in the lower temperature orthorhombic spectra. Using the Debye relaxation model [31], we find that time scale corresponding to the shape and width of the central peak, is a few hundreds femtoseconds for both crystals. Details of modeling the scattering data are presented in the supplemental material.

XRD studies show that both crystals are cubic in the high temperature phase [15, 22]. Factor group analysis of the averaged, cubic structure predicts no Raman activity [32]. The fact that we observe diffuse Raman spectra and the central peak suggests that these structures are highly dynamic, fluctuating among different non-cubic structures in such a way as to appear cubic on average [21].

To learn more about the thermal fluctuations that give rise to the central peak, we measured the angular dependence of cross-polarized Raman spectra [33, 34] of both crystals in the cubic phase (Figure 2a and b). In this experiment, record scattered light polarized perpendicular to the incident light, with incident and scattered light propagating along the direction of the [100] crystal

axis. We repeat this measurement after rotating the linear polarization of the incident light (using a half waveplate) with respect to the crystal surface. In perfectly ordered crystals, the angular modulation of the intensity of scattered light probes the symmetry of an observed mode [33]. In contrast, we probe a central peak that originates from anharmonic, disordered motion. Therefore, the strong and clear angular modulation of the central peak, observed in both CH<sub>3</sub>NH<sub>3</sub>PbBr<sub>3</sub> (Fig. 2a) and CsPbBr<sub>3</sub> (Fig. 2b) is surprising. It indicates that the disordered motion, giving rise to the central peak is highly anisotropic. Even more surprising is that both crystals exhibit similar modulation. This indicates that, although the motion of CH<sub>3</sub>NH<sub>3</sub><sup>+</sup> and Cs<sup>+</sup> are expected to be very different, the modulation of the local polar fluctuations possess similar features for both crystals and must therefore be determined by their common lead-bromide octahedral network. Additionally, though the central peak of both crystals exhibits angular modulation, contrasting Figure 2a with 2b does reveal the effect of the CH<sub>3</sub>NH<sub>3</sub><sup>+</sup> rotation. While CsPbBr<sub>3</sub> exhibits a clear and well-defined minimum in the intensity, CH<sub>3</sub>NH<sub>3</sub>PbBr<sub>3</sub> exhibits a diffuse modulation minimum (see supplemental material for the modulation profile). This non-zero minimum reflects additional isotropic disorder that is induced by CH<sub>3</sub>NH<sub>3</sub><sup>+</sup> rotation, similar to the motion of liquids where the Raman central peak is independent of excitation polarization angle.[35]

To better understand the motions that give rise to the central peak, we performed first-principles MD simulations of CsPbBr<sub>3</sub> at 80 K and 500 K and calculated Raman spectra from the polarizability autocorrelation function of the resulting trajectories [28]. Within this theoretical framework, the connection between Raman central peaks and dynamic local polar order has been established [36, 37]. This can be seen by writing the Raman intensity ( $I$ ) as [37]

$$I^{\mu\nu}(\omega) \propto \int dq' d\omega' \langle P^\mu(r, t) P^\mu(0, 0) \rangle_{q', \omega'} \langle P^\nu(r, t) P^\nu(0, 0) \rangle_{-q', \omega - \omega'} \quad (1)$$

Here,  $\omega$  is Raman frequency,  $q$  is wave vector,  $\langle P^\mu(r, t) P^\mu(0, 0) \rangle$  are polarization-polarization correlation functions, where  $\langle \cdot \rangle$  denotes an average over start times, and  $\mu, \nu$  are cartesian components of  $P$ . A central peak occurs when the line shapes of the polarization-polarization correlation functions are peaked near  $\omega = 0$ , that is, when there are quasi-static temporal correlations occurring over a range of time scales. Using polarizabilities obtained from density functional theory, we calculate Raman spectra that are in good agreement with experiment, showing a strong central peak at 500 K (Fig. 3a).

To obtain insight into the nature of fluctuations giving rise to this central peak, we examine our MD trajectories at 500 K. Root-mean-square displacements (Cs: 0.85

Å, Pb: 0.36 Å, Br: 0.73 Å), as well as typical trajectories (supplemental material), show that Cs is the most mobile atomic species in this material, with Br displaying large fluctuations as well, while Pb is mostly static in comparison. Examination of MD trajectories indicates that instantaneous structures in the cubic phase are characterized by large off-center displacements of the Cs<sup>+</sup> cation as well as tilting and distortions of PbBr<sub>6</sub> octahedra. The angular distribution function of off-center Cs atoms shows that Cs is mainly displaced along the  $\langle 100 \rangle$  directions (supplemental material).

The conditions necessary for a central peak are not only that the structure display large thermal fluctuations, but also that there be incipient polar order, with the stochastic appearance and disappearance of polar motifs. Such temporal behavior gives rise to vibrational response at a continuum of frequencies and a frequency-domain polarization correlation functions and Raman spectra peaked at  $\omega = 0$  (Eq. 1). In contrast, a purely harmonic or weakly anharmonic material will not have spectral weight near  $\omega = 0$ . In CsPbBr<sub>3</sub>, we have found that the polar fluctuations giving rise to the central peak consist primarily of head-to-head motions of Cs atoms, coupled with perpendicular, outward motion of the proximal Br atoms (Fig. 3b). We present evidence for this in the mode-decompositions of frequency-filtered MD trajectories (Fig. 3c). We filter our MD trajectories into frequency intervals of 10 cm<sup>-1</sup> using a band-pass filter, and project these filtered trajectories onto the different Cs modes allowed in our 2×2×2 simulation cell. We find particularly high weight for the modes  $M^8$  ( $\rightarrow\leftarrow$ ), which consist of head-to-head Cs motion (see supplemental material for mode labels), with increasing weight for lower frequencies. A similar analysis for the Br modes shows that motions of Br perpendicular to Pb-Br-Pb bonds dominate the low frequency spectral response (modes labelled as Br<sub>6</sub> rotations and distortions in Fig. 3d). Linear combinations of these modes give rise to concerted outward motion of Br shown in Fig. 3b.

While antiferroelectric modes have been linked to Raman central peaks in other systems [38], the head-to-head motion presented above is a unique aspect of CsPbBr<sub>3</sub>. Such motion is usually thought to be energetically unfavorable due to the opposing dipoles, as may be expected from the prevalence of 180° domain walls over head-to-head domain walls. However, in CsPbBr<sub>3</sub>, the head-to-head Cs motion is stabilized by a cooperative motion of Br as Cs approaches one of the faces of the cubo-octahedral cage. This face, as defined by the positions of the 4 Br on it, tends to expand as this happens. It is energetically favorable for two neighboring Cs to move towards the same face, resulting in head-to-head motion, instead of the two Cs atoms separately causing expansions of two different cubo-octahedron faces. At these short distances, Pauli repulsion interactions dominate Coulomb effects in determining low energy modes. This process is illustrated in animations of the frequency-filtered trajectories and confirmed with further projective

analysis of the MD trajectory (see supplemental material).

The picture of head-to-head motion of Cs atoms is consistent with the  $\pi/2$  period of Raman intensity modulations in our cross-polarized measurements. Furthermore, the strong coupling between Cs and Br fluctuations revealed by the MD simulations is consistent with the pre-resonant Raman effect in CsPbBr<sub>3</sub>, since electronic transitions involve valence band states with strong Br character. The similarities between our CsPbBr<sub>3</sub> and CH<sub>3</sub>NH<sub>3</sub>PbBr<sub>3</sub> pre-resonant Raman spectra suggest a similar picture in CH<sub>3</sub>NH<sub>3</sub>PbBr<sub>3</sub>, with dipolar fluctuations driven by [CH<sub>3</sub>NH<sub>3</sub>]<sup>+</sup>, but strongly coupled to Br motions which experience pre-resonant Raman. Preliminary MD calculations of CH<sub>3</sub>NH<sub>3</sub>PbBr<sub>3</sub> indicate that Br motion does indeed contribute strongly to the central peak, while contributions from [CH<sub>3</sub>NH<sub>3</sub>]<sup>+</sup> motion includes both rotational and displacive components (supplemental material).

Central peaks have been calculated [39] and observed in other systems, such as relaxor materials [40–44], oxide perovskites including BTO [45, 46] and niobates [31, 47–50], and vitreous silica [51, 52]. However, there are differences in the local polar fluctuations of the halide and oxide perovskites arising from structural differences in these systems. Halide perovskites have half the formal charges of the oxide perovskites (*e.g.*, Cs<sup>+</sup>, Pb<sup>2+</sup>, Br<sup>-</sup> vs. Ba<sup>2+</sup>, Ti<sup>4+</sup>, O<sup>2-</sup>), which makes Coulomb and ionic effects much less important in the halides [53]. The larger lattice spacing favors A-site fluctuations in the halide perovskites, while covalence effects due to lone pairs (Pb<sup>2+</sup>, Bi<sup>2+</sup>) favor B-site fluctuations in the oxides. In the oxides, covalency favors dipole alignment due to overbonding effects [54]. On the other hand, Pauli repulsion tends to result in antiferroelectric fluctuations in the halide perovskites via the mechanism discussed above. Thus, the central peaks in the oxides and halides arise from different underlying dynamics.

In conclusion, we compare the low-frequency Raman scattering of CH<sub>3</sub>NH<sub>3</sub>PbBr<sub>3</sub> and CsPbBr<sub>3</sub> crystals in each of their structural phases and show that both systems exhibit significant and surprisingly similar local polar thermal fluctuations in their cubic and tetragonal phases. Thus, the presence of a dipolar organic cation is not a necessary condition for dynamic disorder in the halide perovskites, nor is rotational cation motion. Using MD simulations, we have shown that head-to-head Cs motion coupled to Br face expansion drives dynamic disorder in CsPbBr<sub>3</sub>. In the halide perovskites, the weak bonds between the A-site cation and PbX<sub>3</sub>, together with the stronger bonds within the PbX<sub>3</sub> lattice, produce motion on multiple time scales, which is manifested in the observed diffuse central peak superimposed on the usual sharper features in the Raman spectra.

Structural fluctuations are known to be prevalent in the halide perovskites. Here we precisely identify which vibrational motifs have large amplitude at moderate temperature. In CsPbBr<sub>3</sub>, halide motion, coupled to A-site

translation, is shown to be dominant.  $\text{CH}_3\text{NH}_3\text{PbBr}_3$  shows analogous behavior, with halide motion,  $\text{CH}_3\text{NH}_3$  translation, and  $\text{CH}_3\text{NH}_3$  rotation all contributing to the central peak. Coupling of electronic excitations to these particular motions may deepen understanding of temporal band edge fluctuations [14], carrier localization [7], and dynamical Rashba spin splitting [55, 56].

### Acknowledgments

This work was supported by the U.S. Department of Energy, Office of Science, Office of Basic Energy Sciences, with funding at Columbia University through the Energy Frontier Research Center under Grant No. DE-SC0001085 and at SLAC National Accelerator Laboratory through the AMOS program within the Chemical Sciences, Geosciences, and Biosciences Division. O.Y.

acknowledges funding by the FP7 People program under the project Marie Curie IOF-622653. M.A.P. acknowledges support of the Brazilian Agencies CNPq and Fapemig. L. Z. T acknowledges support of the Office of Naval Research, under grant number N00014-14-1-0761. F. Z. acknowledges support of the DOE Office of BES, under grant number DE-FG02-07ER46431. A. M. R. acknowledges support of the Office of Naval Research, under grant number N00014-12-1-1033. L.K. and D.A.E. were supported by a research grant from Dana and Yossie Hollander, in the framework of the Weizmann Institute of Science (WIS) Alternative Sustainable Energy Research Initiative, AERI. D.A.E. further acknowledges financial support by the Austrian Science Fund (FWF): J3608-N20. MGK acknowledges funding from DOE-NNSA grant and thanks National Nuclear Security Administration for grant DE-NA0002522. We thank Shi Liu for the valuable discussions.

- 
- [1] M. Grätzel, *Nat. Mater.* **13**, 838 (2014).
- [2] H. Zhou, Q. Chen, G. Li, S. Luo, T.-b. Song, H.-S. Duan, Z. Hong, J. You, Y. Liu, and Y. Yang, *Science* (80-. ). **345**, 542 (2014).
- [3] R. J. Worhatch, H. Kim, I. P. Swainson, A. L. Yonkeu, and S. J. L. Billinge, *Chem. Mater.* **20**, 1272 (2008).
- [4] E. Mosconi, C. Quarti, T. Ivanovska, G. Ruani, and F. De Angelis, *Phys. Chem. Chem. Phys.* **16**, 16137 (2014).
- [5] M. A. Carignano, A. Kachmar, and J. Hutter, *J. Phys. Chem. C* **119**, 8991 (2015).
- [6] C. Goehry, G. A. Nemnes, and A. Manolescu, *J. Phys. Chem. C* **119**, 19674 (2015).
- [7] C. Quarti, E. Mosconi, and F. De Angelis, *Phys. Chem. Chem. Phys.* **17**, 9394 (2015).
- [8] J. Even, M. Carignano, and C. Katan, *Nanoscale* **8**, 6222 (2016).
- [9] A. M. A. Leguy, J. M. Frost, A. P. McMahon, V. G. Sakai, W. Kochelmann, C. Law, X. Li, F. Foglia, A. Walsh, B. C. O'Regan, J. Nelson, J. T. Cabral, and P. R. F. Barnes, *Nat. Commun.* **6**, 7124 (2015).
- [10] M. T. Weller, O. J. Weber, P. F. Henry, A. M. Di Pumpo, and T. C. Hansen, *Chem. Commun.* **51**, 4180 (2015).
- [11] J. M. Frost and A. Walsh, *Acc. Chem. Res.* **49**, 528 (2016).
- [12] D. A. Egger, A. M. Rappe, and L. Kronik, *Acc. Chem. Res.* **49**, 573 (2016).
- [13] A. J. Neukirch, W. Nie, J.-C. Blancon, K. Appavoo, H. Tsai, M. Y. Sfeir, C. Katan, L. Pedesseau, J. Even, J. J. Crochet, G. Gupta, A. D. Mohite, and S. Tretiak, *Nano Lett.* **16**, 3809 (2016).
- [14] C. Motta, F. El-Mellouhi, S. Kais, N. Tabet, F. Alharbi, and S. Sanvito, *Nat. Commun.* **6**, 7026 (2015).
- [15] A. Poglitsch and D. Weber, *J. Chem. Phys.* **87**, 6373 (1987).
- [16] A. A. Bakulin, O. Selig, H. J. Bakker, Y. L. A. Rezus, C. Muller, T. Glaser, R. Lovrincic, Z. Sun, Z. Chen, A. Walsh, J. M. Frost, and T. L. C. Jansen, *J. Phys. Chem. Lett.* **6**, 3663 (2015).
- [17] A. Mattoni, A. Filippetti, M. I. Saba, and P. Delugas, *J. Phys. Chem. C* **119**, 17421 (2015).
- [18] A. Mattoni, A. Filippetti, M. I. Saba, C. Caddeo, and P. Delugas, *J. Phys. Chem. Lett.* **7**, 529 (2016).
- [19] I. Chung, J.-H. Song, J. Im, J. Androulakis, C. D. Malliakas, H. Li, A. J. Freeman, J. T. Kenney, and M. G. Kanatzidis, (2012).
- [20] E. L. da Silva, J. M. Skelton, S. C. Parker, and A. Walsh, *Phys. Rev. B* **91**, 144107 (2015).
- [21] C. Quarti, E. Mosconi, J. M. Ball, V. D'Innocenzo, C. Tao, S. Pathak, H. J. Snaith, A. Petrozza, and F. De Angelis, *Energy Environ. Sci.* **9**, 155 (2016).
- [22] C. C. Stoumpos, C. D. Malliakas, J. a. Peters, Z. Liu, M. Sebastian, J. Im, T. C. Chasapis, A. C. Wibowo, D. Y. Chung, A. J. Freeman, B. W. Wessels, and M. G. Kanatzidis, *Cryst. Growth Des.* **13**, 2722 (2013).
- [23] G. Xing, N. Mathews, S. S. Lim, N. Yantara, X. Liu, D. Sabba, M. Grätzel, S. Mhaisalkar, and T. C. Sum, *Nat. Mater.* **13**, 476 (2014).
- [24] P. DiAntonio, B. E. Vugmeister, J. Toulouse, and L. A. Boatner, *Phys. Rev. B* **47**, 5629 (1993).
- [25] R. Farhi, M. E. Marssi, A. Simon, and J. Ravez, *Eur. Phys. J. B - Condens. Matter Complex Syst.* **9**, 599.
- [26] B. E. Vugmeister, *Phys. Rev. B* **73**, 174117 (2006).
- [27] R. Loudon, *Proc. R. Soc. A Math. Phys. Eng. Sci.* **275**, 218 (1963).
- [28] M. Thomas, M. Brehm, R. Fligg, P. Vöhringer, and B. Kirchner, *Phys. Chem. Chem. Phys.* **15**, 6608 (2013).
- [29] H. Mashiyama, Y. Kawamura, H. Kasano, T. Asahi, Y. Noda, and H. Kimura, *Ferroelectrics* **348**, 182 (2007).
- [30] S. Hirotsu, J. Harada, M. Iizumi, and K. Gesi, *J. Phys. Soc. Japan* **37**, 1393 (1974).
- [31] E. Bouziane, M. D. Fontana, and M. Ayadi, *J. Phys. Condens. Matter* **15**, 1387 (2003).
- [32] A. Maalej, Y. Abid, A. Kallel, A. Daoud, A. Lautié, and F. Romain, *Solid State Commun.* **103**, 279 (1997).
- [33] K. Mizoguchi and S.-i. Nakashima, *J. Appl. Phys.* **65**, 2583 (1989).

- [34] H. B. Ribeiro, M. A. Pimenta, C. J. S. de Matos, R. L. Moreira, A. S. Rodin, J. D. Zapata, E. A. T. de Souza, and A. H. Castro Neto, *ACS Nano* **9**, 4270 (2015).
- [35] G. E. Walrafen, M. R. Fisher, M. S. Hokmabadi, and W.-H. Yang, *J. Chem. Phys.* **85**, 6970 (1986).
- [36] V. L. Aksenov, M. Bobeth, N. M. Plakida, and J. Schreiber, *Zeitschrift für Phys. B Condens. Matter* **69**, 393 (1987).
- [37] B. E. Vugmeister, Y. Yacoby, J. Toulouse, and H. Rabitz, *Phys. Rev. B* **59**, 8602 (1999).
- [38] A. K. Tagantsev, K. Vaideeswaran, S. B. Vakhrushev, A. V. Filimonov, R. G. Burkovsky, A. Shaganov, D. Andronikova, A. I. Rudskoy, A. Q. R. Baron, H. Uchiyama, D. Chernyshov, A. Bosak, Z. Ujma, K. Roleder, A. Majchrowski, J.-H. Ko, and N. Setter, *Nat. Commun.* **4**, 2229 (2013).
- [39] I. Grinberg, Y.-H. Shin, and A. M. Rappe, *Phys. Rev. Lett.* **103**, 197601 (2009).
- [40] I. G. Siny, S. G. Lushnikov, R. S. Katiyar, and E. A. Rogacheva, *Phys. Rev. B* **56**, 7962 (1997).
- [41] F. M. Jiang, J.-H. Ko, and S. Kojima, *Phys. Rev. B* **66**, 184301 (2002).
- [42] J.-H. Ko and S. Kojima, *Appl. Phys. Lett.* **91**, 82903 (2007).
- [43] V. K. Malinovsky, A. M. Pugachev, and N. V. Surovtsev, *Bull. Russ. Acad. Sci. Phys.* **74**, 1231 (2010).
- [44] G. Shabbir and S. Kojima, *Ferroelectrics* **303**, 167 (2004).
- [45] V. K. Malinovsky, A. M. Pugachev, V. A. Popova, N. V. Surovtsev, and S. Kojima, *Ferroelectrics* **443**, 124 (2013).
- [46] J.-H. Ko, S. Kojima, T.-Y. Koo, J. H. Jung, C. J. Won, and N. J. Hur, *Appl. Phys. Lett.* **93**, 102905 (2008).
- [47] J. P. Sokoloff, L. L. Chase, and D. Rytz, *Phys. Rev. B* **38**, 597 (1988).
- [48] J. P. Sokoloff, L. L. Chase, and L. A. Boatner, *Phys. Rev. B* **41**, 2398 (1990).
- [49] A. M. Quittet, M. I. Bell, M. Krauzman, and P. M. Raccah, *Phys. Rev. B* **14**, 5068 (1976).
- [50] A. Kania, K. Roleder, G. E. Kugel, and M. D. Fontana, *J. Phys. C Solid State Phys.* **19**, 9 (1986).
- [51] G. Winterling, *Phys. Rev. B* **12**, 2432 (1975).
- [52] U. Buchenau, M. Prager, N. Nücker, A. J. Dianoux, N. Ahmad, and W. A. Phillips, *Phys. Rev. B* **34**, 5665 (1986).
- [53] P. J. Edwardson, L. L. Boyer, R. L. Newman, D. H. Fox, J. R. Hardy, J. W. Flocken, R. A. Guenther, and W. Mei, *Phys. Rev. B* **39**, 9738 (1989).
- [54] E. Cockayne and B. P. Burton, *Phys. Rev. B* **60**, R12542 (1999).
- [55] F. Zheng, L. Z. Tan, S. Liu, and A. M. Rappe, *Nano Lett.* **15**, 7794 (2015).
- [56] T. Etienne, E. Mosconi, and F. De Angelis, *J. Phys. Chem. Lett.* **7**, 1638 (2016).

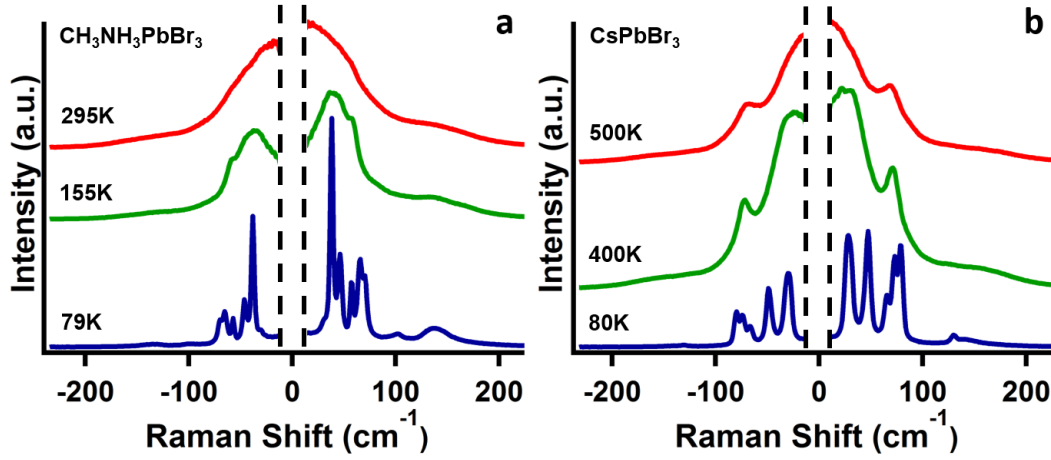


FIG. 1. Low-frequency Raman spectra of hybrid and inorganic lead-halide perovskite crystals. The spectral region obscured by the notch-filter, between  $\pm 10 \text{ cm}^{-1}$  (marked by the vertical dashed lines), has been deleted. (a)  $\text{CH}_3\text{NH}_3\text{PbBr}_3$  and (b)  $\text{CsPbBr}_3$  in the orthorhombic phase (blue), tetragonal phase (green), and cubic phase (red), showing growth of central peak with temperature in both materials.

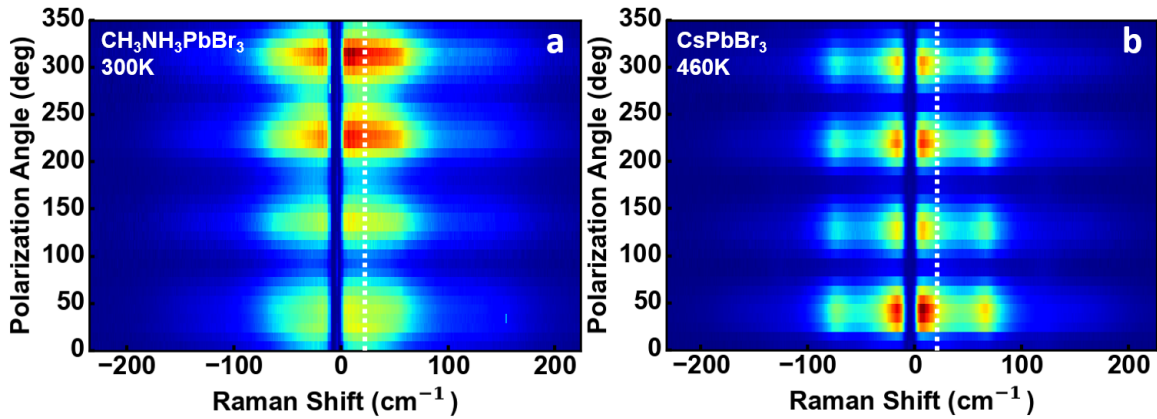


FIG. 2. Cross-polarized low frequency Raman spectra of hybrid and inorganic lead-halide perovskite crystals in the cubic phase, (a)  $\text{CH}_3\text{NH}_3\text{PbBr}_3$  (at 300 K) and (b)  $\text{CsPbBr}_3$  (at 460 K), showing strong polarization angle dependence with  $90^\circ$  period in both materials. The zero of polarization angle is arbitrarily defined. The white dotted line indicates a Raman shift of  $20 \text{ cm}^{-1}$ . The corresponding modulation of the Raman intensity is shown in Fig. S3 in the supplemental material.

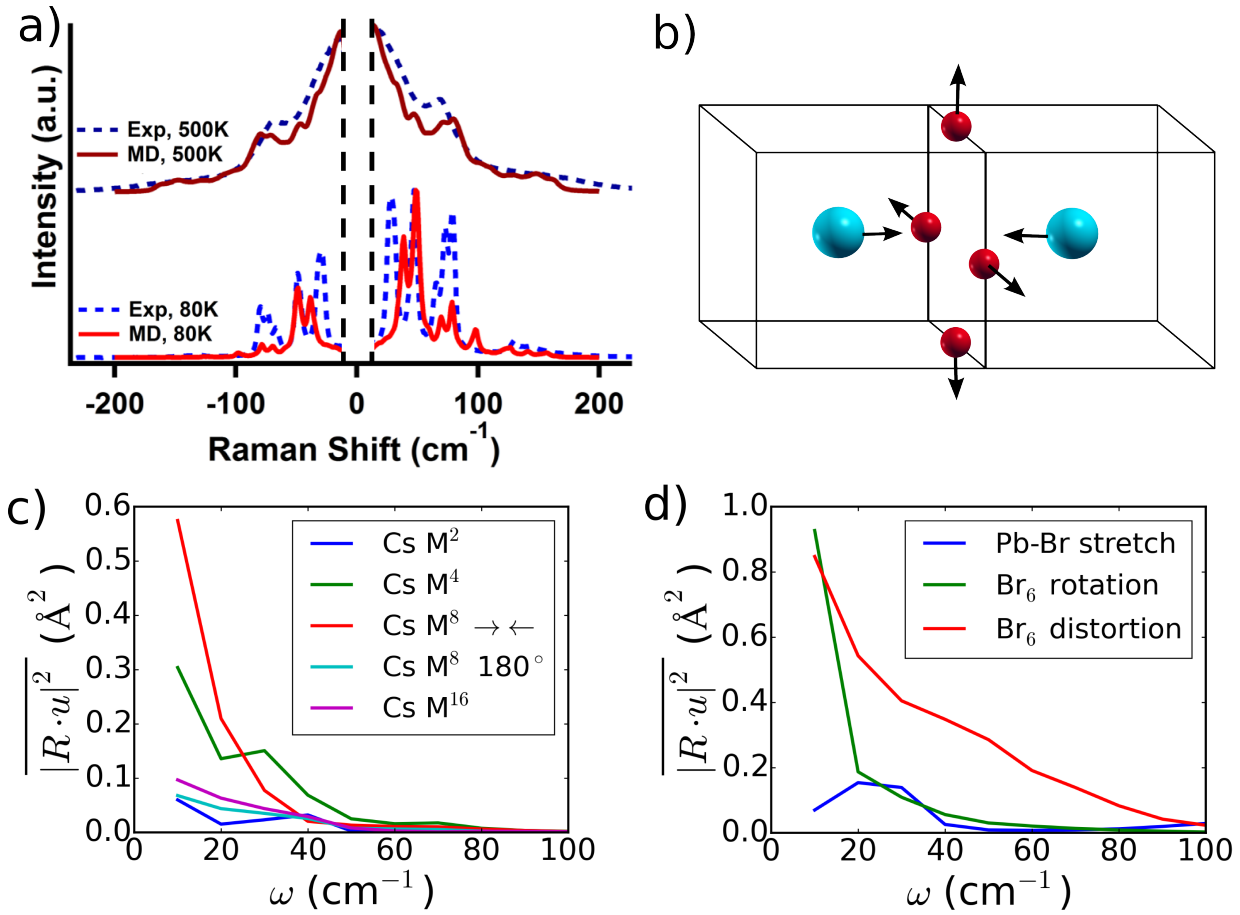


FIG. 3. a) Comparison between MD (solid line) and experimental (dashed line) Raman spectra of CsPbBr<sub>3</sub> at  $T = 80$  K (bottom) and  $T = 500$  K (top). b) Schematic representation of head-to-head Cs motion, coupled with motion of proximal Br, which is responsible for the Raman central peak in CsPbBr<sub>3</sub>. Atoms are colored according to: Cs (cyan), Br (red). c) Projections of frequency-filtered MD trajectories to different Cs modes, categorized by multipole moment (see supplemental material for details). Weights of projections onto different Cs modes are given as a function of frequency of motion. d) Projections of frequency-filtered MD trajectories to different Br modes. Weights of projections onto different Br modes are given as a function of frequency of motion.